

Detection of significant X-ray polarization from transient NS-LMXB XTE J1701–462 with IXPE and its implication on the coronal geometry

Kiran M. Jayasurya^{1*}, Vivek K. Agrawal¹ and Rwitika Chatterjee¹

¹Space Astronomy Group, ISITE Campus, U. R. Rao Satellite Centre, Bangalore, 560037, India

Accepted XXX. Received YYY; in original form ZZZ

ABSTRACT

The first spectro-polarimetric analysis of the transient NS-LMXB XTE J1701 – 462 has been carried out using *IXPE*, *NICER* and *NuSTAR* data during its 2022 outburst. We report the significant detection of energy-dependent polarization in the X-ray signal from the source on 2022 September 29 in the 2 – 4 keV, 4 – 8 keV and 2 – 8 keV energy bands with a polarization degree of $3.9 \pm 0.3\%$ (10.7σ), $5.5 \pm 0.6\%$ (9.1σ) and $4.5 \pm 0.4\%$ (12.6σ), respectively. The polarization angle in the overall 2 – 8 keV band was found to be $\sim 143^\circ \pm 2^\circ$. The spectra were modelled using a combination of thermal emission from an accretion disc, Comptonized emission from the corona and a Gaussian line. From spectro-polarimetric analysis, the polarization degree due to the disc emission was found to have an upper limit of $\sim 6\%$, and that of the Comptonized emission was constrained at $\sim 10.5 \pm 4.9\%$ (at the 3σ level). The implication of these results on the coronal geometry and emission mechanisms is discussed.

Key words: accretion, accretion disks – polarization – X-rays: binaries – X-rays: individual: XTE J1701 – 462

1 INTRODUCTION

Low-mass X-ray binaries (LMXBs) consisting of a low-magnetic field neutron star accreting material from a low-mass companion star show intensity and spectral variations on time scales ranging from hours to months, and are divided into two sub-groups, Z-sources and atoll sources. The classification is based on their joint spectral and temporal nature and the shape of the path that they trace out in the Colour-Colour diagram (CCD) and hardness intensity diagram (HID, [Hasinger & van der Klis 1989](#)). The Z-sources trace out a ‘Z’-shaped track having three branches: horizontal branch (HB), normal branch (NB) and flaring branch (FB). The Z-sources are further classified into two sub-categories based on the extent of their HB and FB. The Cyg-like Z-sources have prominent HB and weak FB, and vice-versa for the Sco-like Z-sources.

XTE J1701 – 462 is a neutron star low-mass X-ray binary (NS-LMXB) discovered with the *All Sky Monitor (ASM)* in January 2006 ([Remillard et al. 2006](#)). The first 10 weeks of observations with the *Rossi X-ray Timing Explorer (RXTE)* suggested that it was a transient Z-source, the first of its kind ([Homan et al. 2007](#)). During the initial high intensity phase, the source displayed Cyg-like behaviour and then evolved into a Sco-like Z-source as the count rate decreased ([Lin et al. 2009](#)). During the decay phase of the ~ 600 days outburst, the source displayed atoll-like behaviour. The source entered a new outburst phase on 2022 September 6 ([Iwakiri et al. 2022](#)).

In general, a combination of a thermal component and a Comptonized emission component is used in modeling the X-ray spectra of Z and atoll sources ([Di Salvo et al. 2000, 2001](#); [Agrawal & Sreekumar 2003](#); [Agrawal & Misra 2009](#); [Agrawal et al. 2023](#); [Tarana et al. 2008](#); [Piraino et al. 2000, 2007](#)). The thermal component is either described by a multi-colour disc component (MCD)

from standard thin disc ([Mitsuda et al. 1984](#)) or a single-temperature blackbody (BB) originating from the boundary-layer/spreading-layer (BL/SL). However, the X-ray spectrum of XTE J1701 – 462 has been fitted with a combination of two thermal components (BB+MCD) and a constrained broken power-law (CBPL) with break energy fixed at 20 keV ([Homan et al. 2007](#); [Lin et al. 2009](#)). Z-sources are generally found in the soft spectral state (SS). In this state, the Comptonized component kT_e is found to be in the range of 2 to 5 keV and the spectrum does not evolve significantly along the complete Z-track ([Di Salvo et al. 2000, 2001, 2002](#); [Agrawal et al. 2020a,b](#); [Agrawal & Misra 2009](#); [Agrawal et al. 2023](#)).

In order to constrain the radiative processes at play and the accretion flow geometry in LMXBs, polarization data in the X-ray band are extremely useful. Some of the LMXBs are a prime target of the *Imaging X-ray Polarimetry Explorer (IXPE)*, a polarimetric mission launched on 2021 December 9 ([Weisskopf et al. 2022](#)). These observations are providing a better view of the physical processes and geometry of the putative corona in these systems ([Capitanio et al. 2022](#); [Farinelli et al. 2022](#); [Chatterjee et al. 2023](#)).

In this letter, we report the detection of polarized X-ray signal from the source using *IXPE* data. We discuss the implication of our results and suggest a possible accretion flow and corona geometry in the source.

2 OBSERVATIONS AND DATA ANALYSIS

2.1 IXPE

IXPE is a Gas Pixel Detector-based soft X-ray imaging polarimeter ([Soffitta et al. 2021](#); [Weisskopf et al. 2022](#)), comprising of a 4 m focal length Mirror Module Assembly focusing X-rays onto three polarization-sensitive detector units (DUs) in the 2 – 8 keV energy

* E-mail: kiranmj@ursec.gov.in

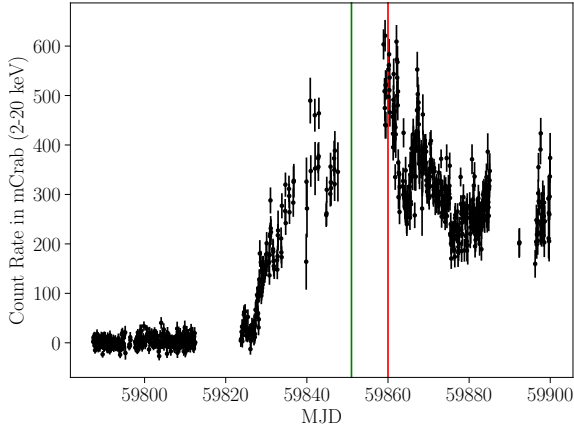


Figure 1. *Maxi/GSC* light curve for XTE J1701 – 462 in the 2 – 20 keV band during the 2022 outburst. The green and the red lines mark the Epoch 1 and Epoch 2 respectively.

range. *IXPE* observed XTE J1701 – 462 on 2022 September (MJD 59851; ObsID 01250601; hereafter referred to as Epoch 1) and again on 2022 October 8 (MJD 59860; ObsID 01250701; hereafter referred to as Epoch 2) for ~ 46.2 ks and ~ 46.4 ks of net exposure times respectively. The *MAXI/GSC* light curve¹ suggested that the source was in the initial high-intensity state of its 2022 outburst (Figure 1).

The processed *IXPE* Level-2 data² was analyzed using IXEPOBSSIM v30.0.0 (Baldini et al. 2022). The source region was defined as a 60" circle and the background region as an annulus of 180" inner and 240" outer radii respectively, centered at the source's centroid intensity. The source and background event lists were extracted using the XPSELECT task, following which the PCUBE algorithm of XPBIN task was used to generate the polarization cubes. The PHA1, PHA1Q and PHA1U algorithms were used to generate the Stokes I, Q and U spectra respectively.

The polarization degree (PD) and polarization angle (PA) were determined using the model-independent PCUBE algorithm (Kislat et al. 2015) for the energy bands 2 – 4 keV, 4 – 8 keV and 2 – 8 keV. The algorithm assumes that the PD and PA are independent, but they are not so in reality, and hence the uncertainties are more appropriately represented by the contours of their joint measurement.

The results of our polarimetric analysis for Epoch 1 are described in Section 3.2. For Epoch 2, we did not find significant polarization, with PD of $0.51 \pm 0.33\%$, $1.60 \pm 0.58\%$, and $0.83 \pm 0.33\%$, for the 2 – 4, 4 – 8 and 2 – 8 keV energy bands respectively, well below the respective minimum detectable polarizations (MDP) at the 99% level. Hence, we did not pursue further analysis for this epoch. We also performed a spectro-polarimetric model-dependent fit (Strohmayr 2017) using XSPEC and the latest *IXPE* response files (v12).

2.2 *NICER* and *NuSTAR*

NICER observed XTE J1701 – 462 on 2022 September 29 (ObsID 5203390122) and 2022 October 9 (ObsID 5203390126) for 465

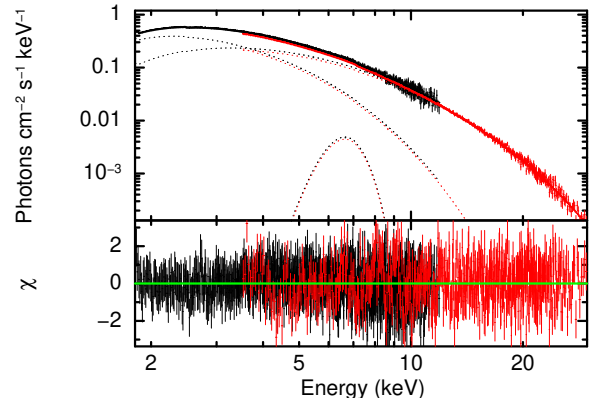


Figure 2. Unfolded X-ray spectra [black: *NICER* (1.8 – 12 keV); red: *NuSTAR* (3.5 – 25 keV)] of the source for Epoch 1 fitted with model 1.

s and 1618 s of net exposure time respectively. The cleaned event files were extracted using *nicer12* task which performs standard calibration and screening of the unfiltered data. The source and background spectra (in the 0.2 – 12 keV energy band) were generated using *nicer13-spect* task. The tasks were performed using *NICER-DAS* software v10 distributed with *HEASOFT* v6.31.1³ and the latest CALDB.

The source was observed by *NuSTAR* on 2022 September 24 (ObsID 90802322004) and 2022 October 8 (ObsID 90801325002) for a net exposure time of 9.34 ks and 12.2 ks respectively. The unfiltered event files were calibrated and screened with the *nupipeline* task of *NuSTARDAS* (v1.9.7) using the latest CALDB files. The spectra in the 3 – 78 keV energy band, and light curves in the 3 – 4.5, 4.5 – 7, 7 – 10.5, and 10.5 – 20 keV energy bands were extracted using the *nuproducts* task.

For Epoch 1, *NICER* ObsID 5203390122 and *NuSTAR* ObsID 90802322004 were considered for deriving the spectral parameters for the spectro-polarimetric fitting with *IXPE* data. The spectra were rebinned to have minimum 25 counts per energy bin. Spectral fitting was done in the 1.8 – 12 keV range for the *NICER* data and 3.5 – 25 keV range for the *NuSTAR* data.

The CCDs for the *NuSTAR* observations were also generated (Figure 3). The soft and hard colours are the ratios of the background-subtracted count rates in the 4.5 – 7 keV & 3 – 4.5 keV, and 10.5 – 20 keV & 7 – 10.5 keV bands, respectively. The source was on the HB and NB of the Z track during Epoch 1, and in the NB and FB during Epoch 2.

3 RESULTS

3.1 Spectral Properties

The *NICER* and *NuSTAR* spectra were fitted with three different models in XSPEC: *tbabs*(diskbb+nthcomp+gaussian)* (hereafter, model 1), *tbabs*(bbodyrad+diskbb+gaussian)* (hereafter, model 2) and *tbabs*(bbodyrad+nthcomp+gaussian)* (hereafter, model 3). All three models produced acceptable fits to the

¹ Public access at <http://maxi.riken.jp/top/slist.html>

² Publicly available on the HEASARC Data Archive

³ <http://heasarc.gsfc.nasa.gov/ftools>

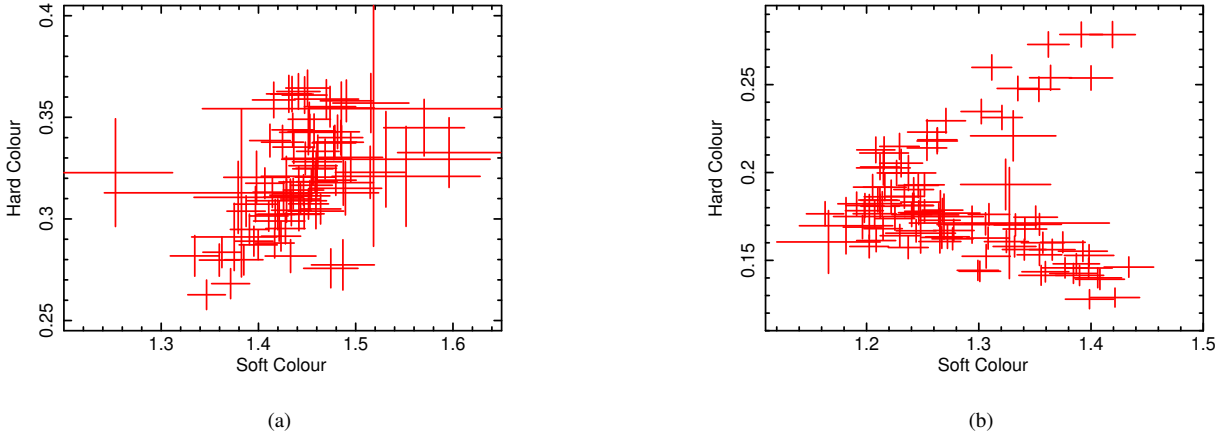


Figure 3. CCDs for *NuSTAR* observations of XTE J1701–462 close to (a) Epoch 1 and (b) Epoch 2. See text for details.

Table 1. Best fit parameters for the fit performed using model 1 for the *NICER* + *NuSTAR* spectrum for Epoch 1. kT_{in} : inner disc temperature (keV); Γ_{nth} : photon index; kT_{bb} : blackbody seed photon temperature (keV); kT_e : plasma temperature (keV). N_{dbb} and N_{nth} are the normalizations of the *diskbb* and *nthcomp* components. E_l , σ_l & N_l are the center, width and normalization of the Gaussian emission line respectively. Hydrogen column density, N_H (10^{22} cm^{-2}) is frozen at best fit value of 1.93. Uncertainties are quoted at 90% confidence interval.

Parameter	Value
kT_{in}	1.22 ± 0.15
N_{dbb}	260.20 ± 80.88
Γ_{nth}	2.48 ± 0.16
kT_e	3.16 ± 0.13
kT_{bb}	1.21 ± 0.10
N_{nth}	0.27 ± 0.11
E_l	6.63 ± 0.09
σ_l	0.69 ± 0.22
N_l	0.008 ± 0.003
χ^2/DOF	1315/1438

Table 2. Polarization parameters obtained using the PCUBE algorithm (for all 3 DUs combined) in different energy bands for Epoch 1. The uncertainties are reported at the 1σ level.

Parameter	2–4 keV	4–8 keV	2–8 keV
Q/I (%)	1.50 ± 0.36	1.04 ± 0.60	1.31 ± 0.36
U/I (%)	-3.58 ± 0.36	5.42 ± 0.60	-4.34 ± 0.36
PD (%)	3.89 ± 0.36	5.52 ± 0.60	4.53 ± 0.36
PA ($^\circ$)	146.39 ± 2.67	140.43 ± 3.14	143.42 ± 2.27

spectra, with χ^2/DOF of 1315/1438, 1323/1440, and 1319/1438 respectively. We find model 1 to be best suited to describe the spectro-polarimetric data during Epoch 1 (see Section 3.2). The broadband (*NICER* + *NuSTAR*) spectrum fitted with this model is shown in Figure 2 and the best-fit parameters are tabulated in Table 1.

3.2 Spectro-Polarimetric Properties

The polarization parameters derived from PCUBE for Epoch 1 are shown in Table 2. The normalized Stokes parameters for the different DUs and with all three DUs combined are also plotted in Figure 4. We note that the source shows significant polarization during this epoch, with PD of 3.89%, 5.52% and 4.53%, (with a significance of 10.7σ , 9.1σ and 12.6σ) for the 2–4, 4–8 and 2–8 keV energy bands respectively. The PA for the respective energy bands are $146.39^\circ \pm 2.67^\circ$, $140.43^\circ \pm 3.14^\circ$, and $143.42^\circ \pm 2.27^\circ$.

We also performed a model dependent spectro-polarimetric analysis by simultaneously fitting the source and background spectra for the different Stokes parameters (I, Q & U) in the different energy bands. This was carried out for the three models described in Section 3.1, multiplied by *polconst* (which assumes a constant PD and PA over the entire energy band), dropping the Gaussian line. The parameters were frozen to their best-fit values, leaving only the normalization and polarization parameters to vary freely. The results of the spectro-polarimetric fit with model 1 are shown in Table 3. Figures 5a and 5b show the 1σ , 2σ , and 3σ contours of this fit in the 2–4, 4–8 and 2–8 keV bands. The polarization parameters and contours, although not fully incident, are in good agreement with those from PCUBE.

We also carried out the spectro-polarimetric analysis with two *polconst*, one multiplied with each component. The polarization of *nthcomp* was well-constrained with PD of 10.5% and PA of $\sim 135.4^\circ$. However, the PD of *diskbb* was unconstrained with a 3σ upper limit on PD at 6.1%. The fit statistic (χ^2/DOF) was found to be 1255/1333. The results are shown in Table 3 and Figure 5c.

For model 2 with multi-*polconst*, the fit statistic was similar at 1256/1333 with *diskbb* PD = $4.95 \pm 1.1\%$ & PA = $147.3^\circ \pm 8.2^\circ$. However, the PD of the *bbodyrad* could not be constrained. For model 3, the PD of *nthcomp* was found to be $4.7 \pm 0.9\%$ and PA of $144.6^\circ \pm 5.7^\circ$. The fit statistic was slightly worse at 1551/1333 and again, the PD of the *bbodyrad* component was unconstrained.

4 DISCUSSION

Though detailed investigations of spectral and temporal properties

⁴ Fitted in the 2–8 keV range

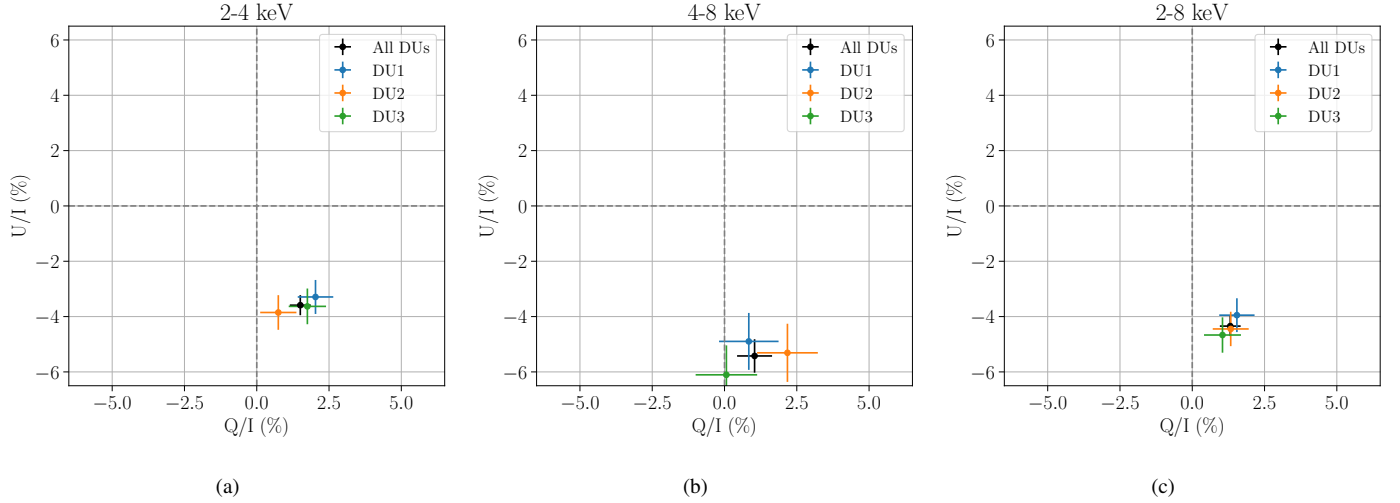


Figure 4. The Q and U Stokes parameters (normalized by Stokes I) derived from PCUBE in the energy bands (a) 2 – 4 keV, (b) 4 – 8 keV, and (c) 2 – 8 keV energy bands, for DU1 (blue), DU2 (orange), DU3 (green) and for the three DUs combined (black). Null polarization corresponds to $(Q/I, U/I) = (0, 0)$.

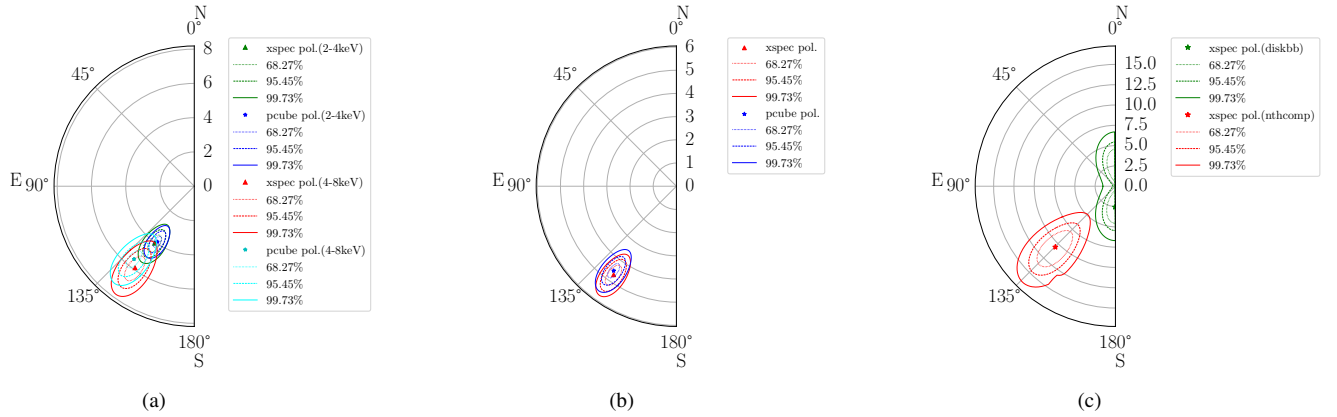


Figure 5. (a) Polarization parameters derived from XSPEC (green and red, triangle and contours) and PCUBE (blue and cyan, star and contours) in the 2 – 4 keV (green & blue) and 4 – 8 keV (red & cyan) energy bands. (b) Polarization parameters derived from XSPEC (red triangle and contours) and PCUBE (blue star and contours) over the 2 – 8 keV energy range. (c) Polarization parameters derived from XSPEC using individual `polconst` for `diskbb` (green star and contours) and `nthcomp` (red star and contours) respectively in the 2 – 8 keV energy range. In all three panels, the *IXPE* spectra have been fitted with the best-fit parameters from model 1 and the 1σ (dotted), 2σ (dashed) and 3σ (solid) contours are shown. See text for details.

Table 3. Polarization parameters derived from the spectro-polarimetric fitting of the Stokes spectra of Epoch 1 in different energy bands using model 1. Uncertainties and upper limit are quoted at the 3σ level. See text for details.

Parameter	Single <code>polconst</code>			Multiple <code>polconst</code> ⁴	
	2-4 keV	4-8 keV	2-8 keV	<code>diskbb</code>	<code>nthcomp</code>
PD (%)	4.05 ± 1.13	5.88 ± 1.62	4.68 ± 0.92	<6.1	10.5 ± 4.9
PA ($^\circ$)	145.2 ± 8.1	144.0 ± 8.0	144.7 ± 5.7	-	135.3 ± 14.0
χ^2/DOF	381/437	854/887	1276/1335		1255/1333

of bright LMXBs have been carried out in the past decades, radiative processes and nature of accretion flow in these systems still remain uncertain. Hence, polarization measurements can play a crucial role in unfolding the nature of accretion flow and emission mechanisms in these sources. XTE J1701 – 462 was in the high intensity state of the 2022 outburst during the *IXPE* observations and was

also observed by *NuSTAR* and *NICER* quasi-simultaneously. During the *NuSTAR* observations, the source traced the HB and NB of the Z-track. The source generally shows Cyg-like behaviour in the high intensity state, and evolves along the complete Z-track over the timescale of a few days. This suggests that the source was probably in the Cyg-like state during Epoch 1. We fitted the *NICER* & *NuSTAR* data (which were ~ 5 days off from each other) and it still results into a good fit, suggesting that the source has not evolved much during this epoch.

In this work, we report the detection of significant X-ray polarization as detailed in Section 3. The measured PD is $4.53 \pm 0.36\%$, $3.89 \pm 0.36\%$ and $5.52 \pm 0.60\%$ in the 2 – 8, 2 – 4 and 4 – 8 keV band respectively and the PA is found to be $\sim 143^\circ$ (Ref. Table 2). We also carried out model dependent analysis of spectro-polarimetric data using three different models. The application of model 3 to the spectro-polarimetric data gives a worse fit compared to model 1 and model 2 (see Section 3.2). Model 2 provides good fit to the

IXPE data and indicates that the disc emission is polarized. However, in this case the blackbody emission is found to be unpolarized. The blackbody emission mainly contributes in the energy band > 5 keV. However, a strong polarization signature has been observed in 4–8 keV using model-independent analysis. Model 1 also produces good fit to the spectro-polarimetric data. We note that the PA obtained by fitting the spectro-polarimetric data with this model 1 is in accordance (within error) with that obtained using model independent analysis. Hence, it is likely that model 1 is a better approach to describe the X-ray spectra of the bright LMXBs.

The orbital inclination of the system is $\sim 70^\circ$ (Lin et al. 2009). During the observations, the source was in the soft state. The simulations carried out by Gnarini et al. (2022) suggests that the PA should be greater than 120° for a slab-like geometry for a system in soft spectral state, and with inclination of 70° . Their simulations also suggest that for this geometry, the PD should increase with increasing energy, which is in the accordance with our findings. Hence, we propose that a thick slab-like corona above the inner part of the disc, obscuring emission from the NS surface, is responsible for the Comptonized radiation. Such a corona is cool ($kT_e \sim 3$ keV), optically thick ($\tau_{\text{slab}} \sim 4$) and located between the NS surface and inner part of accretion disc, probably covering some fraction of inner disc as well.

A radio jet like emission in the north-south direction had been observed in this source (Fender et al. 2007). However, recent MeerKAT and ATCA observations of its new outburst suggest that the large-scale jet could have probably been a background feature (Gasealahwe et al. 2022, priv. com. with Prof. Rob Fender). Hence, we cannot comment about the orientation of PA of the polarized X-ray signal with respect to the symmetry axis.

ACKNOWLEDGMENTS

The authors thank GH, SAG; DD, PDMSA and Director, URSC for encouragement and continuous support to carry out this research.

This research used data products provided by the *IXPE* team (MSFC, SSDC, INAF, and INFN) and software tools distributed by the High-Energy Astrophysics Science Archive Research Center (HEASARC), at NASA Goddard Space Flight Center (GSFC).

DATA AVAILABILITY

IXPE, *NICER* and *NuSTAR* data underlying this work are available at High Energy Astrophysics Science Archive Research Center (HEASARC) facility, located at NASA-Goddard Space Flight Center. The MAXI light curve used in this work is publicly available at <http://maxi.riken.jp/top/slist.html>.

REFERENCES

- Agrawal V. K., Misra R., 2009, *MNRAS*, **398**, 1352
 Agrawal V. K., Sreekumar P., 2003, *MNRAS*, **346**, 933
 Agrawal V. K., Nandi A., Ramadevi M. C., 2020a, *Ap&SS*, **365**, 41
 Agrawal V. K., Nandi A., Ramadevi M. C., 2020b, *Ap&SS*, **365**, 56
 Agrawal V. K., Nandi A., Katoch T., 2023, *MNRAS*, **518**, 194
 Baldini L., et al., 2022, *SoftwareX*, **19**, 101194
 Capitanio F., et al., 2022, *arXiv e-prints*, p. [arXiv:2212.12472](https://arxiv.org/abs/2212.12472)

- Chatterjee R., Agrawal V. K., Jayasurya K. M., Katoch T., 2023, *arXiv e-prints*, p. [arXiv:2301.13394](https://arxiv.org/abs/2301.13394)
 Di Salvo T., et al., 2000, *ApJ*, **544**, L119
 Di Salvo T., Robba N. R., Iaria R., Stella L., Burderi L., Israel G. L., 2001, *ApJ*, **554**, 49
 Di Salvo T., Robba N., Stella L., 2002, *Mem. Soc. Astron. Italiana*, **73**, 1082
 Farinelli R., et al., 2022, *Monthly Notices of the Royal Astronomical Society*, **519**, 3681
 Fender R. P., Dahlem M., Homan J., Corbel S., Sault R., Belloni T. M., 2007, *MNRAS*, **380**, L25
 Gasealahwe K., Motta S. E., van den Eijnden J., Russell T., Fender R., Miller-Jones J., Woudt P., Monageng I., 2022, *The Astronomer's Telegram*, **15617**, 1
 Gnarini A., Ursini F., Matt G., Bianchi S., Capitanio F., Cocchi M., Farinelli R., Zhang W., 2022, *MNRAS*, **514**, 2561
 Hasinger G., van der Klis M., 1989, *A&A*, **225**, 79
 Homan J., et al., 2007, *ApJ*, **656**, 420
 Iwakiri W., et al., 2022, *The Astronomer's Telegram*, **15592**, 1
 Kislat F., Clark B., Beilicke M., Krawczynski H., 2015, *Astroparticle Physics*, **68**, 45
 Lin D., Remillard R. A., Homan J., 2009, *ApJ*, **696**, 1257
 Mitsuda K., et al., 1984, *PASJ*, **36**, 741
 Piraino S., Santangelo A., Kaaret P., 2000, *A&A*, **360**, L35
 Piraino S., Santangelo A., di Salvo T., Kaaret P., Horns D., Iaria R., Burderi L., 2007, *A&A*, **471**, L17
 Remillard R. A., Lin D., ASM Team at MIT NASA/GSFC 2006, *The Astronomer's Telegram*, **696**, 1
 Soffitta P., et al., 2021, *The Astronomical Journal*, **162**, 208
 Strohmayer T. E., 2017, *ApJ*, **838**, 72
 Tarana A., Bazzano A., Ubertini P., 2008, *ApJ*, **688**, 1295
 Weisskopf M. C., et al., 2022, *Journal of Astronomical Telescopes, Instruments, and Systems*, **8**, 026002

This paper has been typeset from a $\text{\TeX}/\text{\LaTeX}$ file prepared by the author.